Talanta 135 (2015) 94–101

Contents lists available at ScienceDirect

Talanta

journal homepage: www.elsevier.com/locate/talanta

Ni(II)NTA AuNPs as a low-resource malarial diagnostic platform for the rapid colorimetric detection of *Plasmodium falciparum* Histidine-Rich Protein-2

Christopher P. Gulka, Joshua D. Swartz, David W. Wright*

Department of Chemistry, Vanderbilt University, Station B 351822-1822, Nashville, TN 37235-1822, United States

ARTICLE INFO

Article history:
Received 13 October 2014
Received in revised form
23 December 2014
Accepted 29 December 2014
Available online 7 January 2015

Keywords:
Ni(II)NTA
Gold nanoparticles
Malaria
Low-resource diagnostics
Histidine-Rich Proteins
Smartphone technology

ABSTRACT

Diagnosing infectious diseases remains a challenge in the developing world where there is a lack of dependable electricity, running water, and skilled technicians. Although rapid immunochromatographic tests (RDTs) have been deployed to diagnose diseases such as malaria, the extreme climate conditions encountered in these regions compounded with the discrepancies in test manufacturing have yielded varying results, so that more innovative and robust technologies are sought. Devoid of antibodies and thermally sensitive materials, we present a robust, colorimetric diagnostic platform for the detection of a malarial biomarker, *Plasmodium falciparum* Histidine-Rich Protein 2 (*Pf*HRP-II). The assay exploits the optical properties of gold nanoparticles, covalently coupling them to a Ni(II)NTA recognition element specific for *Pf*HRP-II. In the presence of the recombinant malarial biomarker (rcHRP-II), the Ni(II)NTA AuNPs begin to crosslink and aggregate in as little as one minute, triggering a red-to-purple color change in solution. To increase assay sensitivity and platform stability suitable for low-resource regions, the Ni(II)NTA AuNPs were assembled with varying spacer ligands in a mixed monolayer presentation. When assembled with a negatively charged Peg_4-thiol ligand, the Ni(II)NTA AuNPs demonstrate low nanomolar limits of rcHRP-II detection in physiological concentrations of human serum albumin and maintain excellent stability at 37°C when stored for four weeks. Detection of the malaria biomarker is also measured by capturing and processing images of aggregated gold nanoparticles with a smartphone camera. By utilizing a smartphone camera and image processing application, there is no significant difference in assay sensitivity and rcHRP-II limit of detection in comparison to a spectrophotometer, further making this diagnostic platform applicable for use in low-resource regions.

1. Introduction

In the developing world, early, rapid, and accurate diagnosis is essential to control epidemics and curb resistance for diseases such as tuberculosis, HIV/AIDS, and malaria. Unfortunately, high healthcare costs in these regions compounded with a lack of reliable electricity, a lack of skilled technicians, and a minimal infrastructure burdens disease diagnosis. For malaria, a parasitic disease that threatens most of the developing world each year, rapid point-of-care diagnostic devices are necessitated. In order to combat diagnosis issues presented in the developing world, immunochromatographic rapid diagnostic strip tests (RDTs) have been distributed to detect malarial infection in as little as 15–30 min by capturing *Plasmodium falciparum* malarial parasitic antigens in patient blood samples [1]. In 2011, the World Health Organization (WHO) implemented an assessment of these strip tests and determined that only 20% retained the 200–2000 parasites/μL threshold range in patient blood samples recommended by the WHO [2]. One of the primary explanations for test failure included antibody degradation from long-term storage in the extreme climates encountered in low-resource regions. As a result, innovative, sensitive, and robust approaches for antigen recognition are necessitated for accurate malaria diagnosis.

Upon infection, the *Plasmodium falciparum* parasite secretes 97% of its synthetic biomarker protein, Histidine-Rich Protein-2 (*Pf*HRP-II), into the host's blood, offering an attractive biomarker for disease diagnosis [3]. However, recent discoveries have revealed that *P. falciparum* strains in Senegal and India have exhibited genetic diversity, and polymorphisms in the *Pf*HRP-II antigen have been discovered, further complicating diagnosis via immunoassay platforms [4,5]. Approximately ~85% of the primary structure of *Pf*HRP-II is comprised of AHH and AHHAAD repeats, so that targeting these histidine subunit repeats offers an alternative approach for molecular recognition [6]. Ni(II)Nitrilotriacetic acid

* Corresponding author. Tel.: +1 615 322 2636; fax: +1 615 322 1234.
E-mail address: david.wright@vanderbilt.edu (D.W. Wright).

http://dx.doi.org/10.1016/j.talanta.2014.12.047
0039-9140/

(NTA) chelation has been well established as a strategy to extract and isolate His-tagged proteins, and this octahedral organometallic complex retains micromolar affinity to histidine by coordinating two amino acid subunits per molecule [7–10]. Considering *Pf*HRP-II is a naturally occurring His-tagged protein, Ni(II)NTA complexes have the potential to coordinate multiple repeats per protein.

The coupling of a Ni(II)NTA recognition component to a more robust and sensitive platform would alleviate many of the aforementioned issues with existing RDTs. Colloidal gold nanoparticles offer a desirable signal transduction approach because of their unique optical properties and biologically inert surface. In the presence of visible light, the electrons at the AuNP particle surface oscillate in-phase with the incident radiation, so that monodisperse colloids exhibit a narrow localized surface plasmon resonance (LSPR) band in the visible spectrum, thus transmitting bright red colors in solution. The LSPR signal is sensitive to changes in the dielectric environment encompassing the particles, inspiring applications in both sensor and diagnostic development. Shifting the LSPR band can be induced by the physical aggregation of as little as 2–10 particles, which ultimately triggers a color change in solution [11–13]. Although the gold surface is understood to be biologically inert, colloidal gold nanoparticles are well known for their facile ligand coupling via covalent Au–thiol chemistry, providing a robust and stable interface capable of enduring the extreme climates typically found in South America, sub-Saharan Africa, and southern Asia where malaria is endemic [14]. By exploiting these properties, colloidal gold nanoparticles have been well established as aggregation-induced colorimetric sensors for detection of nucleic acids, proteins, small molecules, and metal ions [15–19].

In this investigation, we aim to create a robust, low-resource colorimetric indicator for malaria diagnosis by selectively and rapidly aggregating Ni(II)NTA AuNPs only in the presence of a recombinant *Pf*HRP-II (rcHRP-II) biomarker, triggering a spectrophotometric redshift and subsequently, a red-to-purple color change (Fig. 1). A custom, thiolated Ni(II)NTA recognition ligand has been previously synthesized and validated in our lab as a proof-of-concept design with Ni(II)NTA Au and AgNPs by detecting histidine-rich peptide mimics [20]. However, the activity of Ni(II)NTA AuNPs has never been assessed against *Pf*HRP-II and the limits of detection for the peptide mimics are outside of the clinically relevant range for malaria diagnosis. We also aspire to optimize the AuNP platform with varying spacer ligands for enhanced signal and stability, along with validating the diagnostic utility of these particles in a complex physiological matrix, mimicking patient samples. In addition, smartphones are emerging as rapid detection technologies in the medical industry, especially through the use of high dynamic range cameras and image processing applications. The rapid colorimetric detection of explosives, pH, and disease biomarkers has been previously detected and analyzed using smartphone technology and processing [21–24]. The ability to capture a color image of aggregated nanoparticles with a smartphone and subsequently analyze the respective signal intensity using an application would reduce user bias and aid in low-resource diagnosis of infectious diseases.

2. Experimental

2.1. Materials and reagents

Citrate-stabilized gold nanoparticles (15 nm) were purchased from Ted Pella, Inc. Thiol-dPeg$_4$-acid (Peg$_4$) was purchased from Quanta Biodesign, Ltd. Recombinant *P. falciparum* Histidine-Rich Protein-II (rcHRP-II) was purchased from CTK Biotech. The thiolated NTA recognition ligand was synthesized previously in our lab. 11-Mercaptoundecanoic acid (MUA) and 6-mercaptohexanol (MHOL) were both purchased from Sigma-Aldrich. The confounding proteins, human serum albumin (HSA) and glutathione-S-transferase (GST), were purchased from Sigma-Aldrich. All other materials/buffers were purchased from either Sigma-Aldrich or Fisher Scientific. All deionized water was used with a resistivity greater than 18 MΩ cm^2.

2.2. Instrumentation and equipment

UV–vis spectra were taken with an Agilent 8453 spectrophotometer with a photodiode array detector. Spectrophotometric assays were performed in Corning 384 well plates and measured with a Biotek Synergy H4 plate reader. Electron microscopy images were taken with a CM 20 transmission electron microscope at 200 kV. A Malvern Zetasizer was utilized for in-solution dynamic laser light scattering size distribution measurements. An Eppendorf 5415D microcentrifuge was used to centrifuge AuNPs in 1.5 mL Eppendorf tubes. A Thermo Reciprocal Shaking Bath was utilized to store the particles at 37°C. Photographs of suspended Ni(II)NTA AuNPs were taken with an iPhone 4S smartphone (Apple, CA).

2.3. Synthesis of Ni(II)NTA AuNPs

A 2 nM aliquot of 15 nm citrate-stabilized AuNPs was incubated with 5 μM thiolated NTA ligand and 5 μM spacer ligand and allowed to assemble on the particle surface overnight. For synthesis of the 100% Ni(II)NTA AuNPs, 10 μM thiolated NTA ligand was incubated with the particles and assembled overnight. The next morning 1 mL aliquots of NTA-functionalized AuNPs were washed by centrifugation at 7200*g* for 45 min. The supernatant was removed and the particles were resuspended in

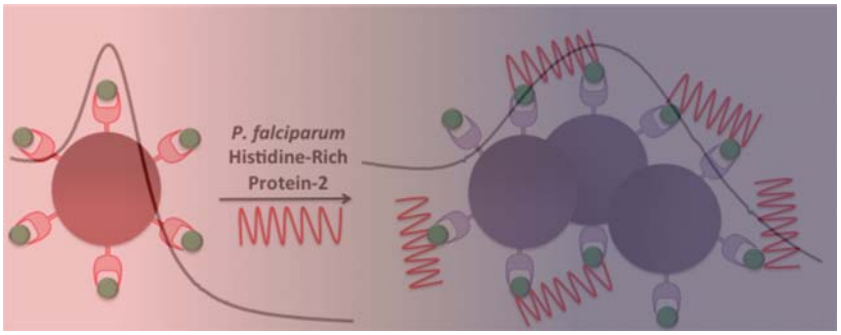

Fig. 1. Color change of Ni(II)NTA AuNPs upon aggregation induced by rcHRP-II. (For interpretation of the references to color in this figure legend, the reader is referred to the web version of this article.)

0.1 M 4-(2-hydroxyethyl)-1-piperazineethanesulfonic acid (HEPES) buffer containing 0.025% Tween 20 (pH 7.4). This process was repeated three additional times and finally suspended in 0.1 M HEPES containing 0.025% Tween 20 (pH 7.4). Next, 10 μM $NiCl_2$ was added to the particles and incubated for 24 h. After charging with Ni^{2+}, the particles were washed three times with 0.1 M HEPES buffer containing 0.025% Tween 20 (pH 7.4). After decanting the final supernatant, the particles were suspended in 0.1 M 2-(N-morpholino) ethanesulfonic acid (MES) buffer containing 0.025% Tween 20 (pH 5.5). The particles were finally filtered through a 0.22 μm syringe filter.

2.4. rcHRP-II-induced aggregation assays with Ni(II)NTA AuNPs

A 5 μL volume of rcHRP-II dissolved in deionized water was mixed with a 45 μL volume of 1.15 nM AuNPs in a Corning 384 well plate. The plate was shaken for 15 min before taking absorbance measurements at 600 nm and 525 nm for Ni(II)NTA AuNPs. A blank measurement consisted of 45 μLs of 0.1 M MES with 0.025% Tween 20 (pH 5.5) plus 5 μL deionized water. After the blank was subtracted, the aggregation signal was assessed by taking the ratio of the two selected wavelengths (A_{600}/A_{525}) and normalizing the samples containing no protein to 1. All measurements were performed in triplicate, while 6 replicates of blank measurements were recorded. All limit of detection values were generated as follows: $(\text{blank}+3\sigma_{\text{blank}})/\text{slope}$.

2.5. rcHRP-II-induced aggregation assays with Ni(II)NTA AuNPs in human serum albumin

A 5 μL volume of rcHRP-II dissolved in 37 mg/mL HSA was mixed with a 45 μL volume of 1.15 nM Peg_4:Ni(II)NTA AuNPs in a Corning 384 well plate. Particles were suspended in 0.1 M MES buffer containing 125 mM imidazole and 150 mM NaCl with 0.025% Tween 20 (pH 5.5). The plate was shaken for 15 min before taking absorbance measurements at 600 nm and 525 nm for Ni(II)NTA AuNPs. A blank measurement consisted of 45 μLs of 0.1 M MES in 125 mM imidazole and 150 mM NaCl with 0.025% Tween 20 (pH 5.5) plus 5 μL 37 mg/mL human serum albumin. After the blank was subtracted, the aggregation signal was assessed by taking the ratio of the two selected wavelengths (A_{600}/A_{525}) and normalizing the samples containing no rcHRP-II to 1. All measurements were performed in triplicate, while 6 replicates of blank measurements were recorded.

2.6. Low-resource Ni(II)NTA AuNP aggregation analysis with iOS application

The Peg_4:Ni(II)NTA AuNPs were titrated against rcHRP-II in a white Costar 96 well plate. A 180 μL Peg_4:Ni(II)NTA AuNP suspension (1.15 nM) in 0.1 M MES containing 125 mM imidazole and 150 mM NaCl with 0.025% Tween 20 (pH 5.5) was added to a white Costar 96 well plate. Next, 20 μLs of a rcHRP-II protein solution was added to the wells before incubating for 15 min. High dynamic range images of the AuNPs were captured with an iPhone 4S camera with the iOS 7.0.6 platform. For color analysis, the commercially available iPhone application, Color Companion (Digital Media Interactive, LLC), was downloaded onto the iOS 7.0.6 platform for analysis of the red, blue and green signal intensities of nanoparticle suspensions in each well. Analysis was calculated by averaging the green and blue signal intensities and dividing it by the red signal intensity. Blank measurements (no protein added to wells) were normalized to values of one.

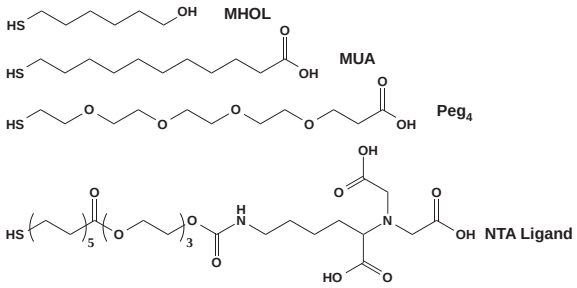

Fig. 2. Ligands assembled onto nanoparticles in this investigation.

3. Results and discussion

3.1. Ni(II)NTA AuNP characterization

The functionalization of gold nanoparticles with a thiolated Ni(II) NTA recognition ligand specific for the *Pf*HRP-II malarial biomarker has the potential to create a rapid, robust diagnostic, capable of withstanding the extreme climates encountered in low-resource regions of the world. Moreover, manipulation of the gold particle surface with varying spacer ligands has the ability to improve both assay sensitivity and long-term stability in the developing world. The spacer ligands addressed in this study are shown in Fig. 2. The alkanethiols, mercaptoundecanoic acid (MUA) and mercaptohexanol (MHOL) possess strong self-assembly characteristics because the van der Waals interactions between methylene units on neighboring ligands promote a strong and stable monolayer adsorbed to the gold surface [25]. MUA contains a terminal negative charge, enhancing stability of colloidal particles, while MHOL possesses a terminal alcohol, facilitating crosslinking interactions and hydrogen bonding between the protein–particle interface. Thiol-$dPEG_4$-Acid (Peg_4) also possesses a terminal negative charge, but possesses hydrophilic character, promoting favorable interactions among aqueous colloidal nanomaterials. In addition, poly(ethylene glycol) molecules are well-known for their anti-fouling and repellant properties versus protein and cell adsorption, further enhancing stability and reducing the risk of non-specific binding [26–29]. Upon functionalization with 50:50 ratios of Ni(II)NTA recognition ligand relative to varying spacer ligands, the particles are stable, as indicated by the bright red colors in solution, the narrow surface plasmon resonance band in the UV–vis spectra, and the monodisperse particle size distribution in the electron microscopy images (Fig. 3). Relative to citrate-stabilized gold nanoparticles, the Ni(II)NTA-functionalized particles undergo a 3–5 nm redshift in the UV–vis spectrum, which correlates to the coordination of a dielectric monolayer to the particle surface, as indicated by the 3–5 nm hydrodynamic diameter increase in laser light scattering experiments (S1).

3.2. Ni(II)NTA AuNP aggregation induced by rcHRP-II

Our previous Ni(II)NTA Au and AgNP platform demonstrating the aggregation activity of *Pf*HRP-II peptide mimics highlights the importance of pH in the assay. Below the isoelectric point of histidine (~6), the positively charged free imidazole side chains create a hydrogen bond network among neighboring proteins, thus facilitating crosslinking interactions between the Ni(II)NTA moieties on neighboring particles and the protein. In addition, below pH 7, *Pf*HRP-II primarily adopts a α-helical structure *in vitro*, orienting histidine units on the surface of the protein [30]. *Pf*HRP-II was also discovered to coordinate as many as 15–17 Fe(II) heme molecules *in vitro* via bishistidyl axial ligation, ultimately adopting a 3_{10}-helical secondary structure in the process [31]. The slightly acidic pH nature of the assay gives rise to protein orientations for favorable Ni(II)-histidine coordination and reduced steric effects,

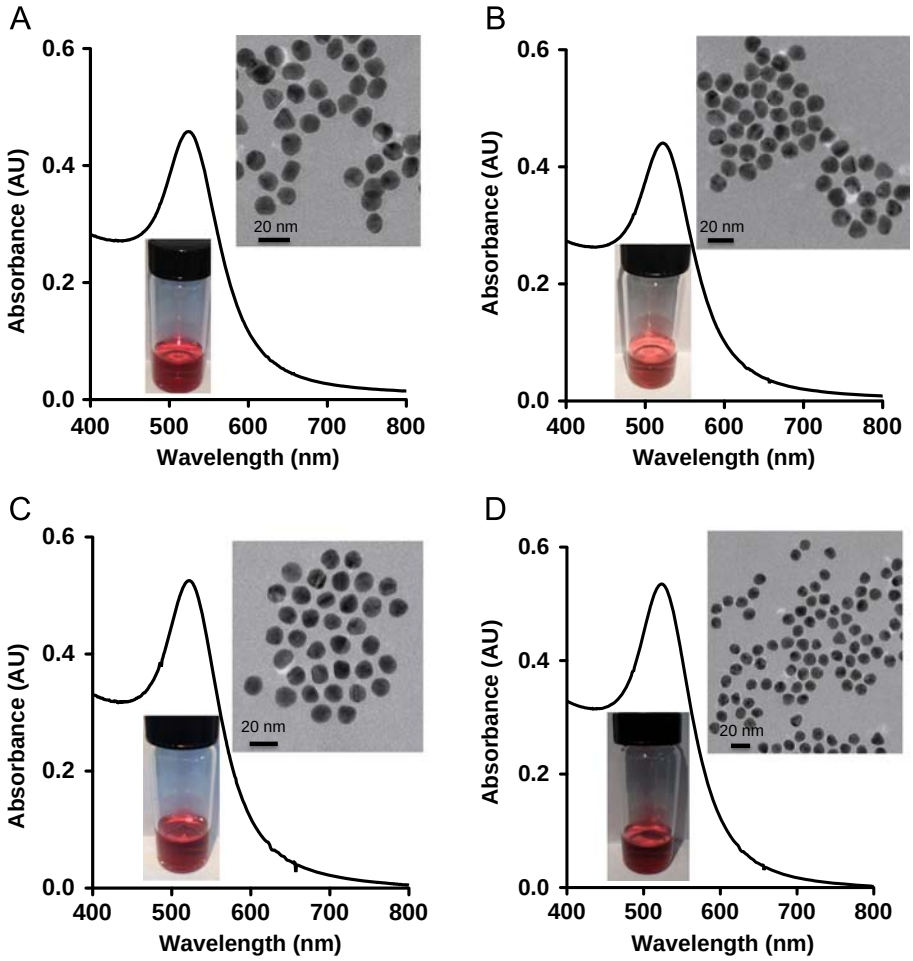

Fig. 3. Ni(II)NTA AuNP Characterization in 0.1 M MES with 0.025% Tween 20 (pH 5.5). UV–vis spectra, TEM images and suspended AuNP images of monodisperse (A) 100% Ni(II)NTA AuNPs, (B) 50:50 MHOL:Ni(II)NTA AuNPs, (C) 50:50 Peg_4:Ni(II)NTA AuNPs, and (D) 50:50 MUA:Ni(II)NTA AuNPs. (For interpretation of the references to color in this figure legend, the reader is referred to the web version of this article.)

while the heme binding studies validate M(II) affinity as a recognition component. Upon reacting the Ni(II)NTA AuNPs with 100 nM rcHRP-II at pH 5.5, all particles exhibit rapid aggregation. Indicated by the significant spectrophotometric redshift, the particles physically change color from red to purple, due to plasmon band coupling from rcHRP-II-induced aggregation (Fig. 4). Protein-induced aggregation is further confirmed by TEM images and the substantial shift in size distribution of particles in dynamic laser light scattering experiments. Nearly 50% of the spectrophotometric signal given off by particle aggregation occurs after one minute, as indicated by a substantial redshift in the UV–vis spectra (S2). Final absorbance measurements are taken after 15 min, as the spectrophotometric signal begins to level off. The rapid timeframe required to generate a signal induced by particle aggregation compares very well with the 15–30 min timeframe for current RDT's.

In order to determine the activity of the Ni(II)NTA AuNPs with varying spacer ligands, rcHRP-II is titrated against each Ni(II)NTA AuNP platform (Fig. 5). After 15 min incubation with rcHRP-II, the spectrophotometric signal is measured by taking a ratio of two selected absorbance wavelengths ($A_{600\ nm}/A_{525\ nm}$) and normalizing the blank values to 1. With the assembly of all spacer ligands, the assay limit of detection increases by an order of magnitude relative to the 100% Ni(II)NTA AuNPs (Table 1). The MHOL:Ni(II)NTA AuNPs exhibit the highest sensitivity along with the largest signal-to-noise at the saturated rcHRP-II concentrations. Contrastingly the 100% Ni(II)NTA AuNPs display the lowest sensitivity, signal-to-noise, and the highest limit of rcHRP-II detection. The Peg_4:Ni(II)NTA AuNPs and MUA:Ni(II)NTA AuNPs exhibit excellent limits of detection, but decreased signal and sensitivity in comparison to MHOL:Ni(II)NTA AuNPs. It is hypothesized that steric crowding of the 100% Ni(II)NTA ligand monolayer is responsible for the poor sensitivity and detection limits. When Ni(II)NTA AuNPs are assembled with MUA and Peg_4 spacer ligands, the terminal negative charge on the spacer ligand most likely repels the particles, decreasing their overall signal and sensitivity relative to the MHOL:Ni(II)NTA AuNPs. The assembly of Ni(II)NTA AuNPs with the small MHOL reduces steric crowding and its terminal alcohol facilitates hydrogen-bonding interactions among the protein–particle interface, ultimately favoring aggregation in the presence of rcHRP-II. Compared to the high nanomolar limits of detection against histidine-rich peptide mimics, the Ni(II)NTA AuNP platform assembled with spacer ligands increases the rcHRP-II limits of detection by two orders of magnitude into clinically relevant ranges.

3.3. *Ni(II)NTA AuNP stability*

To determine the environmental suitability of the Ni(II)NTA AuNPs as a malarial diagnostic, the particles with varying spacer ligands are evaluated in conditions mimicking low-resource settings. All of the particles are stored in assay conditions in a water bath (37°C) for a four-week time period, mimicking low-resource regions with the most extreme temperatures and humidity. At two-week and four-week intervals, the aggregation activity of

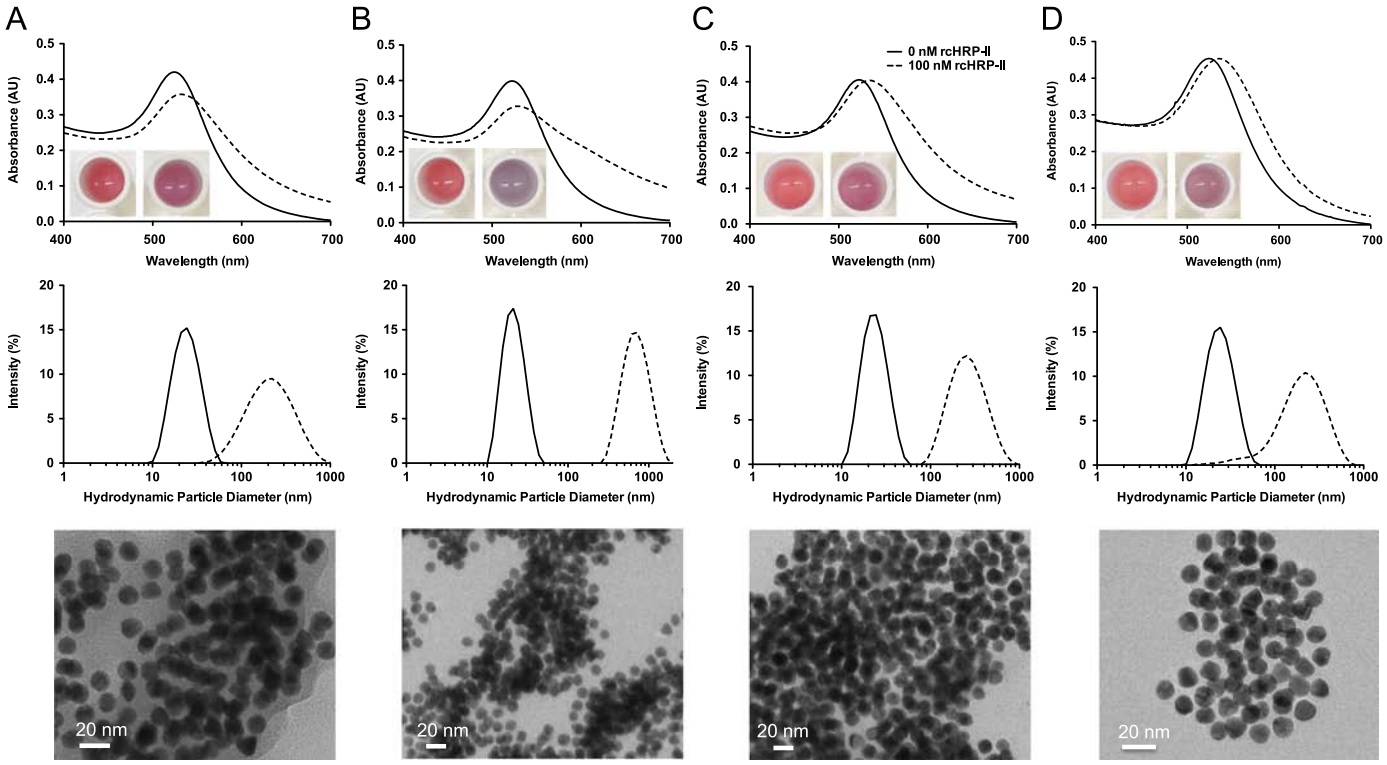

Fig. 4. Aggregation of Ni(II)NTA AuNPs in the presence of 100 nM rcHRP-II at pH 5.5 for (A) 100% Ni(II)NTA AuNPs, (B) 50:50 MHOL:Ni(II)NTA AuNPs, (C) 50:50 Peg_4:Ni(II)NTA AuNPs, and (D) 50:50 MUA:Ni(II)NTA AuNPs. The top graphs represent UV–vis spectra before (solid line) and after (dashed line) adding rcHRP-II. The images on the left are the color changes the particles undergo before (left) and after (right) aggregation. The middle graphs represent dynamic laser light scattering particle size distributions before (solid line) and after (dashed line) rcHRP-II-induced aggregation. The bottom row shows TEM images of rcHRP-II-induced aggregated Ni(II)NTA AuNPs. (For interpretation of the references to color in this figure legend, the reader is referred to the web version of this article.)

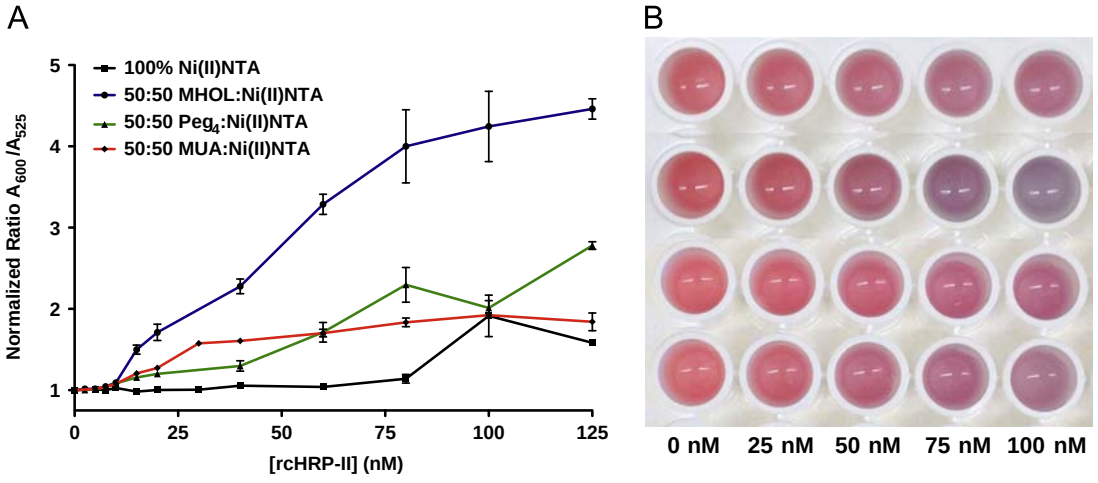

Fig. 5. Titration of rcHRP-II with Ni(II)NTA AuNPs assembled with varying spacer ligands in 0.1 M MES with 0.025% Tween 20 (pH 5.5). (A) Spectrophotometric titrations and (B) Colorimetric titrations ranging from 0–100 nM rcHRP-II concentrations. From top, 100% Ni(II)NTA AuNPs, 50:50 MHOL:Ni(II)NTA AuNPs, 50:50 Peg_4:Ni(II)NTA AuNPs, and 50:50 MUA:Ni(II)NTA AuNPs.

Table 1
LODs, confidence intervals, and sensitivity of rcHRP-II with each Ni(II)NTA AuNP platform in 0.1 M MES buffer containing 0.025% Tween 20 (pH 5.5).

Ni(II)NTA AuNP Platform	LOD (nM)	95% LOD CI (nM)	Sensitivity (Signal/nM)	95% Sensitivity CI (Signal/nM)
100% Ni(II)NTA	51	39–60	0.0066	0.0050–0.0082
50:50 MHOL:Ni(II)NTA	6.6	2.4–10	0.040	0.036–0.045
50:50 Peg_4:Ni(II)NTA	7.4	2.8–11	0.015	0.013–0.017
50:50 MUA:Ni(II)NTA	6.7	5.2–8.0	0.021	0.019–0.024

the particles is assessed upon exposure to 100 nM rcHRP-II (Fig. 6). Ni(II)NTA AuNPs assembled with the negatively charged MUA and Peg_4 spacer ligands maintain consistent aggregation activity over the four-week time period. We hypothesize that the stable self-assembled monolayer along with the negative terminal charge prevents particle aggregation in solution in order to maintain stability. In addition, the 100% Ni(II)NTA AuNPs also preserve stability at the elevated temperature because the Ni(II)NTA complex is partially negatively charged. In contrast, the MHOL: Ni(II)NTA AuNPs lose approximately two-third of their aggregation

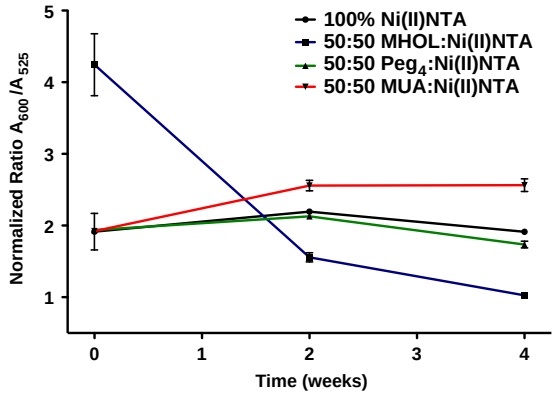

Fig. 6. Stability of Ni(II)NTA AuNPs at 37°C. 1 nM Ni(II)NTA AuNP suspensions at pH 5.5 are stored in sealed 1.5 mL Eppendorf tubes in a water bath at 37°C for four weeks. At two-week intervals, the particles are reacted with 100 nM rcHRP-II for 15 min before taking absorbance measurements at 525 nm and 600 nm.

activity after two weeks and nearly 100% activity after four weeks. It has been recently understood that colloidal AuNPs assembled with short-chained alkanethiols lose stability due to their overwhelming van der Waal interactions between neighboring ligands, and aggregation ultimately occurs [32]. This study also affirms that colloidal AuNPs assembled with longer MUA and Peg_4 ligands retain stability. The AuNP stability is further tracked by measuring variances in the UV–vis spectra at the aforementioned time intervals. The LSPR peak associated with the MHOL:Ni(II)NTA AuNPs begins to redshift after one week at 37°C. After four weeks elapsed time, these particles lose significant absorbance in the UV–vis spectrum, and the LSPR redshifts approximately 65 nm, indicating complete aggregation and a lack of stability in these conditions (S3) and (S4). Contrastingly, the 100% Ni(II)NTA AuNPs and MUA:Ni(II)NTA AuNPs maintain $>80\%$ of their LSPR absorbance after four weeks, while the Peg_4:Ni(II)NTA AuNPs possess $>90\%$ of their LSPR absorbance after four weeks.

3.4. Peg_4:Ni(II)NTA AuNP assay performance in Human serum albumin

Peg_4:Ni(II)NTA AuNPs were chosen for further assays in human serum albumin (HSA) complex matrices because of their consistent stability and activity when stored at elevated temperatures. The Peg_4:Ni(II)NTA AuNPs retain the highest relative LSPR peak absorbance after four weeks incubation in addition to their consistent aggregation activity at 37°C. Moreover, Peg molecules are well established as anti-fouling agents, further reducing non-specific binding in our assay. A series of blocking conditions is first established for the Peg_4:Ni(II)NTA AuNPs. Imidazole is known to have millimolar affinity to Ni(II)NTA and serves as a blocking agent to physiological confounding proteins such as HSA [33]. When incubated in 0.1 M MES buffer containing imidazole and NaCl, the Peg_4:Ni(II)NTA AuNPs are stable up to 250 mM concentrations, whereas above 250 mM imidazole, the Ni(II)NTA sites become overwhelmed by imidazole, and aggregation ultimately occurs. In the presence of 100 nM rcHRP-II, imidazole enhances assay performance linearly from 0 mM to 50 mM imidazole. Between 50 mM and 250 mM imidazole, the maximum assay signal plateaus, whereas above 250 mM, assay signal decreases due to the lack of stability of the Ni(II)NTA AuNPs (S5). A blocking condition of 125 mM imidazole was chosen because at this concentration, the signal-to-noise ratio is optimized and the particles are monodisperse. The particles are first titrated against rcHRP-II and demonstrate a three-fold increase in sensitivity and a two-fold signal-to-noise enhancement (Table 2). The protonated imidazole

Table 2
LODs, confidence intervals, and sensitivity of rcHRP-II using a Peg_4:Ni(II)NTA AuNP platform with 125 mM imidazole and 150 mM NaCl blocking conditions in 0.1 M MES with 0.025% Tween 20 (pH 5.5) in varying concentrations of a physiological confounding protein, human serum albumin.

[HSA] (mg/mL)	LOD (nM)	95% LOD CI (nM)	Sensitivity (Signal/nM)	95% Sensitivity CI (Signal/nM)
37	2.9	1.5–4.1	0.074	0.067–0.082
0	4.2	0.24–7.0	0.053	0.040–0.067

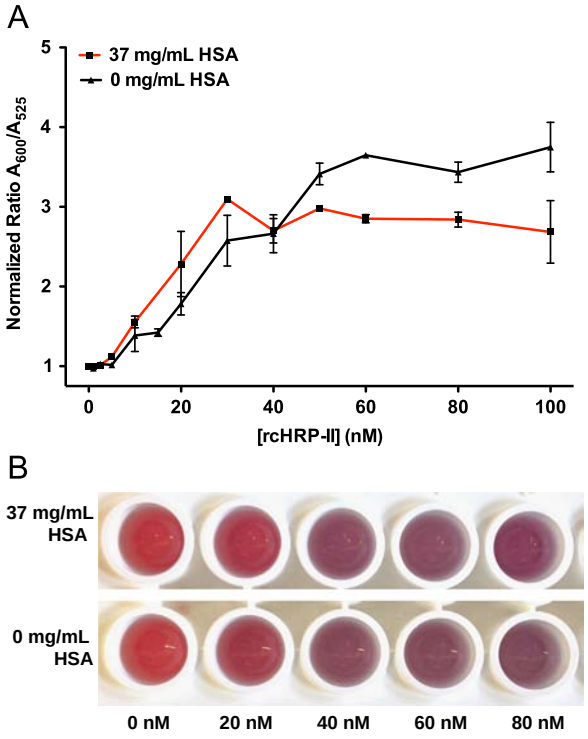

Fig. 7. Effect of Peg_4:Ni(II)NTA AuNP rcHRP-II-induced aggregation in the presence of the physiological confounding protein, HSA. Particles are suspended in 0.1 M MES containing 125 mM imidazole and 150 mM NaCl with 0.025% Tween 20 (pH 5.5). A 45 μL volume of AuNPs is reacted with 5 μL of rcHRP-II for 15 min before taking (A) absorbance measurements and (B) capturing the color changes of rcHRP-II-induced aggregated AuNPs.

cations at high concentrations aid in rcHRP-II-induced Ni(II)NTA AuNP aggregation by facilitating the cation–hydrogen bond network among neighboring proteins, thus increasing assay sensitivity. To control for non-specific interactions, the Ni(II)NTA AuNPs are titrated against the fusion protein tagged onto rcHRP-II, glutathione-S-transferase (GST), and no significant aggregation is evident (S6). The Peg_4:Ni(II)NTA AuNPs are also stable in plasma as indicated by the lack of a UV–vis spectral shift (S8), demonstrating that no physiological confounding proteins induce non-specific aggregation.

In order to mimic a potential patient sample, rcHRP-II is dissolved in the physiological concentrations of HSA, 37 mg/mL. Upon titration, the Peg_4:Ni(II)NTA AuNP colorimetric assay has the same sensitivity versus 0 mg/mL HSA, as demonstrated by the spectrophotometric linear dynamic range and the similar color change upon reactions with rcHRP-II (Fig. 7). There is also no significant difference in limits of detection when rcHRP-II is dissolved in 37 mg/mL versus 0 mg/mL HSA, demonstrating the robust nature of the Peg_4:Ni(II)NTA AuNP platform (Table 2). The

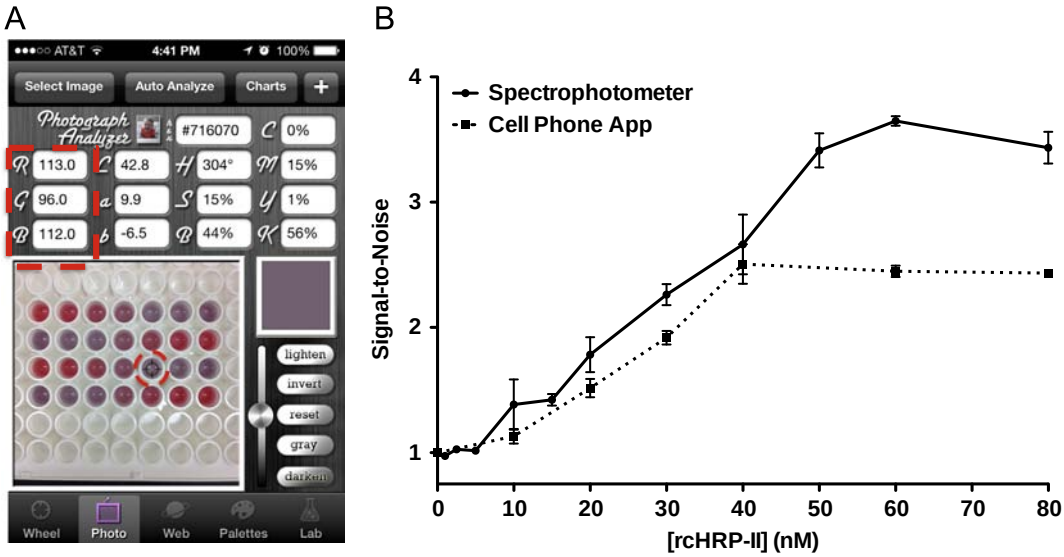

Fig. 8. Workflow of low-resource detection of rcHRP-II using the Peg_4:Ni(II)NTA AuNP platform. (A) The Peg_4:Ni(II)NTA AuNPs were titrated with rcHRP-II and after 15 min, images of the suspended particles were captured with an iPhone 4S camera and uploaded into the Color Companion commercial application. In order to process the color change induced by rcHRP-II, the bullseye cursor (highlighted with the dashed red circle) was moved over a well in a white 96 well-plate and RGB signal intensities were conferred (highlighted with the dashed red box). To calculate raw signal, the green and blue signal intensities were averaged and divided by the red signal intensity values. (B) Plot of signal intensity measured with a spectrophotometer and the Color Companion commercial application. There is no significant difference in sensitivity and rcHRP-II limit of detection between the spectrophotometer and the commercial application.

125 mM imidazole concentration provides adequate blocking in the complex biological matrix, but does not interfere with rcHRP-II-induced aggregation when dissolved in 37 mg/mL HSA. The low nanomolar limits of detection are competitive with the WHO's upper threshold limit of detection of 2000 parasites/μL, which corresponds to approximately 1 nM *Pf*HRP-II. The Peg_4:Ni(II)NTA AuNP platform is also optimized for long-term exposure in low-resource environments and is equipped for utility in complex biological matrices.

3.5. *Peg_4:Ni(II)NTA AuNP colorimetric analysis with smartphone application*

Although Peg_4:Ni(II)NTA AuNP activity can be easily measured with a spectrophotometer in a laboratory setting, the lack of trained technicians coupled with the inconsistent electricity burdens this analytical technique in low-resource regions. However, the physical color transitions of Peg_4:Ni(II)NTA AuNP aggregates upon rcHRP-II incubation can be captured with a battery-powered iPhone and subsequently quantified with image processing applications, further making this diagnostic platform applicable to low-resource areas. Taking advantage of a commercially available iPhone application, Color Companion, photographs of suspended nanoparticles are uploaded and processed for analysis of the RGB color intensities. To achieve a raw signal intensity value, the blue and green intensities are averaged and divided by the red intensity value. The rcHRP-II biomarker is titrated with the Peg_4:Ni(II)NTA AuNPs in a white 96 well plate for enhanced contrast (S9). The wells containing AuNPs with no protein added are normalized to values of one. The signal generated by the Color Companion application yields a linear response between 0 and 40 nM rcHRP-II concentrations before saturation, similar to the signal generated by a spectrophotometer (Fig. 8). There is also no significant difference between the sensitivity (0.038 Signal/nM) and limit of detection (5.2 nM) in comparison to spectrophotometric detection. The image capturing and processing using this smartphone platform are capable of processing and quantifying molecular recognition events in future colorimetric assays.

4. Conclusion

In this investigation, we optimized the Ni(II)NTA AuNP platform for detection of a malarial biomarker, recombinant *Pf*HRP-II, by incorporating various spacer ligands onto the surface for maximum stability and sensitivity. With the negatively charged, water-soluble Peg_4 spacer ligand assembled to the particle surface, the Ni(II)NTA AuNPs retain excellent stability when stored at 37°C for four weeks, demonstrating that this diagnostic platform can endure the harsh climates encountered in low-resource regions. In the presence of rcHRP-II, the Ni(II)NTA AuNPs aggregate in as little as one minute, while the 15-min timeframe required to level the spectrophotometric signal is very competitive with existing malaria RDTs. The Peg_4:Ni(II)NTA AuNPs also exhibit low nanomolar limits of rcHRP-II detection when dissolved in the physiological concentration of the most abundant confounding protein, human serum albumin, overlapping the WHO's upper threshold detection limit of 2000 parasites/μL. Finally, the aggregated AuNPs are photographed with an iPhone camera and processed with a commercially available application, demonstrating similar sensitivity and limits of detection in comparison to a spectrophotometer. Although the optimized Ni(II)NTA AuNP colorimetric indicator displays adequate specificity and sensitivity towards Histidine-Rich Proteins in minimally confounding matrices, establishing similar signals in blood and plasma remains a challenge. Future investigation is required in order to interface this detection strategy with our sample preparation device in order to purify and concentrate the *Pf*HRP-II biomarker from complex matrices for enhanced sensitivity and specificity [33]. Nevertheless, the simple user interface of this diagnostic platform coupled with the rapid response times of rcHRP-II-induced AuNP aggregation makes this assay amenable to low-resource settings.

Acknowledgments

Funding was graciously provided by the Bill and Melinda Gates Foundation (OPP1028749). The authors would also like to thank M. F. Richards for critical comments concerning the manuscript. The

authors would finally like to thank the Color Companion application developers at Digital Media Interactive, LLC.

Appendix A. Supporting information

Supplementary data associated with this article can be found in the online version at http://dx.doi.org/10.1016/j.talanta.2014.12.047.

References

[1] C.K. Murray, R.A. Gasser Jr., A.J. Magill, S.A. Miller, Clin. Microbiol. Rev. 21 (2008) 97–110.
[2] WHO. World Malaria Report, 2011.
[3] P.L. Chiodini, K. Bowers, P. Jorgensen, J.W. Barnwell, K.K. Grady, J. Luchavez, A.H. Moody, A. Cenizal, D. Bell, Trans. R. Soc. Trop. Med. Hyg. 101 (2007) 331–337.
[4] N. Wurtz, B. Fall, K. Bui, A. Pascual, M. Fall, C. Camara, B. Diatta, K.B. Fall, P.S. Mbaye, Y. Dieme, R. Bercion, B. Wade, S. Briolant, B. Pradines, Malar. J. 12 (2013) 34–41.
[5] N. Kumar, J.P.N. Singh, V. Pande, N. Mishra, B. Srivastava, R. Kapoor, N. Valecha, A.R. Anvikar, Malar. J. 11 (2012) 298–304.
[6] L.J. Panton, P. Mcphie, W.L. Maloy, T.E. Wellems, D.W. Taylor, R.J. Howard, Mol. Biochem. Parasitol. 35 (1989) 149–160.
[7] K. Terpe, Appl. Microbiol. Technol. 60 (2003) 523–533.
[8] S. Mori, H.K. Takahashi, K. Yamaoka, M. Okamoto, M. Nishibori, Life Sci. 73 (2003) 93–102.
[9] P. Ghimire, J.C. Samantaray, B.R. Mirdha, A.K. Patra, A.K. Panda, Southeast Asian J. Trop. Med. Public Health 34 (2003) 739–743.
[10] S. Knecht, D. Ricklin, A.N. Eberle, B. Ernst, J. Mol. Recognit. 22 (2009) 270–279.
[11] U. Kreibig, L. Genzel, Surf. Sci. 156 (1985) 678–700.
[12] M. Quinten, U. Kreibig, Surf. Sci. 172 (1986) 557–577.
[13] E. Prodan, P.J. Nordlander, J. Chem. Phys. 120 (2004) 5444–5454.
[14] H. Hakkinen, Nat. Chem. 4 (2012) 443–455.
[15] R. Elghanian, J.J. Storhoff, R.C. Mucic, R.L. Letsinger, C.A. Mirkin, Science 277 (1997) 1078–1081.
[16] J.J. Storhoff, R. Elghanian, R.C. Mucic, C.A. Mirkin, R.L. Letsinger, J. Am. Chem. Soc. 120 (1998) 1959–1964.
[17] F. Xia, X. Zuo, R. Yang, Y. Xiao, D. Kang, A. Vallée-Bélisle, X. Gong, J.D. Yuen, B.B.Y. Hsu, A.J. Heeger, K.W. Plaxco, Proc. Nat. Acad. Sci. 107 (2010) 10837–10841.
[18] J. Liu, Y. Lu, J. Am. Chem. Soc. 125 (2003) 6642–6643.
[19] E. Boisselier, D. Astruc, Chem. Soc. Rev. 38 (2009) 1759–1782.
[20] J.D. Swartz, C.P. Gulka, F.R. Haselton, D.W. Wright, Langmuir 27 (2011) 15330–15339.
[21] L. Shen, J.A. Hagen, I. Papautsky, Lab Chip 12 (2012) 4240–4243.
[22] V. Oncescu, D. O'Dell, D. Erickson, Lab Chip 13 (2013) 3232–3238.
[23] S. Lee, V. Oncescu, M. Mancuso, S. Mehtac, D. Erickson, A Smartphone, Lab Chip 14 (2014) 1437–1442.
[24] J.W. Oh, W.J Chung, K. Heo, H.E. Jin, B.Y. Lee, E. Wang, C. Zueger, W. Wong, J. Meyer, C. Kim, S.Y. Lee, W.G. Kim, M. Zemla, M. Auer, A. Hexemer, S.W. Lee, Nat. Commun. 5 (2014) 3043–3050.
[25] J.C. Love, L.A. Estroff, J.K. Kriebel, R.G. Nuzzo, G.M. Whitesides, Chem. Rev. 105 (2005) 1103–1169.
[26] K.L. Prime, G.M. Whitesides, Science 252 (1991) 1164–1167.
[27] K.L. Prime, G.M. Whitesides, J. Am. Chem. Soc. 115 (1993) 10714–10721.
[28] K. Bandyopadhyay, L. Shu, H. Liu, L. Echegoyen, Langmuir 16 (2000) 2706–2714.
[29] I. Banerjee, R.C. Pangule, R.S. Kane, Adv. Mater. 23 (2011) 690–718.
[30] C.E. Benedetti, J. Kobarg, T.A. Pertinhez, R.M. Gatti, O.N. de Souza, A. Spisni, R. Meneghini, Mol. Biochem. Parasitol. 128 (2003) 157–166.
[31] E.L. Schneider, M.A. Marletta, Biochemistry 44 (2005) 979–986.
[32] H. Hinterworth, S. Kappel, T. Waitz, T. Prohaska, W. Lindner, M. Lammerhofer, ACS Nano 7 (2013) 1129–1136.
[33] K.M. Davis, J.D. Swartz, F.R. Haselton, D.W. Wright, Anal. Chem. 84 (2012) 6136–6142.